# OBSERVATION OF CHF PHENOMENA BASED ON A VISUALIZATION OF NEAR WALL BOILING STRUCTURE IN A VERTICAL NARROW CHANNEL SUBMERGED IN A POOL

**In-Cheol Chu[*], Dong Jin Euh, and Chul-Hwa Song**
Korea Atomic Energy Research Institute
989-111 Daedeok-daero, Yuseong-gu, Daejeon, 305-353, Korea
chuic@kaeri.re.kr; djeuh@kaeri.re.kr; chsong@kaeri.re.kr

## ABSTRACT

We visualized and identified a high heat flux boiling structure in a vertical narrow channel submerged in a pool of saturated R-113. A transparent ITO (Indium Tin Oxide) sputtered sapphire substrate was used as a heating surface and a Pyrex glass plate was placed in parallel to the sapphire substrate to form a gap of 2.25 mm between two vertical plates. Synchronized visualizations were applied to capture the complicated bubble motion and the corresponding dynamic behavior of dry areas on the boiling surface. A total reflection was used to visualize the dry pattern of the boiling surface, and a shadowgraph was used to visualize the bubble motion in a narrow channel. The experiments covered the heat flux condition ranging from 30.9% CHF (critical heat flux) to CHF condition. Above the heat flux of about 77% CHF condition, a slug bubble was periodically formed and the base of the slug bubble became mostly dry. However, the large dry area under the slug bubble was efficiently rewetted by the slug tail region as the slug bubble moved upward. The cooling of the heating surface was governed by the rewetting efficiency of the slug tail region which deteriorated gradually with an increase of the heat flux. CHF occurred when the dry area formation capability in the slug tail region overwhelmed the rewetting capability of the slug tail region.

**KEYWORDS**
Critical heat flux, vertical pool boiling, local boiling structure, total reflection, shadowgraph

## 1. INTRODUCTION

Since Nukiyama [1] discovered the boiling curve and CHF phenomena, a lot of studies have been carried out to identify the CHF triggering mechanism over the past five decades. As a result, a number of theoretical models and CHF mechanisms have been proposed for various boiling systems (*i.e.*, pool and flow boiling systems; horizontal, vertical, and inclined boiling surfaces). Most of these CHF models and mechanisms were developed based on a hypothetical boiling structure and/or visualization of a global boiling structure [2-9].

Advancement in the visualization of a local boiling structure on a heating surface at high heat flux condition has been made in the past twenty years. The dynamic behavior of dry areas or phase distribution on the heating surface were observed by the total reflection technique [10-13] and DEPIcT [14]. An instantaneous two-dimensional temperature distribution of a boiling surface was measured using infrared thermometry [15, 16]. These studies reported that the key physics of the CHF triggering mechanism was the dynamic behavior of the dry area under a massive bubble hovering on a surface and the appearance of

---

[*] Author to whom correspondence should be addressed.

a non-rewetting dry area. However, these studies focused on the high heat flux boiling structure and CHF phenomena of a horizontal heating surface in a pool.

Some research reactors and marine ship reactors adopt a plate-type nuclear fuel assembly. The gap between parallel vertical fuel plates ranges from 2 to 3 mm, typically for research reactors. In addition, boiling in a confined narrow channel is encountered in high-performance heat exchangers and electronics component cooling. The CHF value for a vertical plate in a pool is strongly affected by the existence of the narrow confinement [17]. However, the studies to identify the local boiling structure on a heating surface and CHF mechanism for this kind of geometry are quite lacking.

In this study, CHF phenomena as well as global and local boiling structures near a heating surface were observed for a vertical narrow channel submerged in a pool, using the total reflection and shadowgraph visualization techniques.

## 2. EXPERIMENTAL APPARATUS AND METHOD

The present experimental apparatus consisted of a boiling pool with a vertical transparent heating surface, a DC power supply, a data acquisition system, light sources, and two synchronized high speed video cameras. The overall configuration of the apparatus is similar to the previous works of Chu et al. [12, 13], but the main difference is that the boiling pool and the heating surface is vertically oriented. The boiling pool had a cubic shape, and it had a dimension of 200 mm × 105 mm × 115 mm (height × width × depth). A reflux condenser was installed at the top of the boiling pool. The pressure of the pool was maintained at atmospheric pressure. Two auxiliary cartridge heaters were inserted from the bottom part of the pool to maintain the pool at a saturated temperature condition. Two thermocouples were inserted from the side wall of the pool to measure the pool temperature. A photo of the boiling pool is presented in Fig. 1. Freon R-113 was used as a boiling fluid.

A rectangular sapphire substrate was placed at the center of the back side wall of the pool (Fig. 2). The area and thickness of the sapphire substrate were 80 × 120 mm$^2$ and 1 mm, respectively. A 350 nm thick electro-conductive transparent ITO (Indium Tin Oxide) layer was sputtered on the center of the sapphire substrate, and the ITO layer was used as a heating source for the present boiling experiments. The effective heating length of the ITO layer was 44.5 mm, and the width of the ITO layer in this region was 10 mm (Fig. 3). A Pyrex glass plate is placed in front of the sapphire substrate, forming a 2.25 mm narrow gap between them. The Pyrex plate is 30 mm wide, 120 mm long, and 1 mm thick.

The main visualization methods were a total reflection and a shadowgraph. Two identical high speed video cameras, NAC Memrecam GX-3, were used. One was for the total reflection, and the other was for the shadowgraph (Fig. 2). The cameras were synchronized within ±0.05 msec, using an external TTL signal. Xenon HID lamps were used as light sources for both visualization methods. The camera and lamp for the total reflection were aligned close to the critical angle of the Snell's law. For the shadowgraph, the camera and the lamp were located at the back side and at the front side of the sapphire substrate, respectively. A prism-shaped Pyrex block was attached to the sapphire substrate where the ITO layer was sputtered in order to accommodate the total reflection at the boiling surface.

The total reflection is probably the most effective way to observe the dynamic behavior of the dry areas formed under the bubbles on the boiling surface because the dry areas under the bubbles appear bright and the regions wetted by liquid appear dark in the total reflection image. The basic principle of the total reflection is explained in more detail in the works of Chu et al. [12].
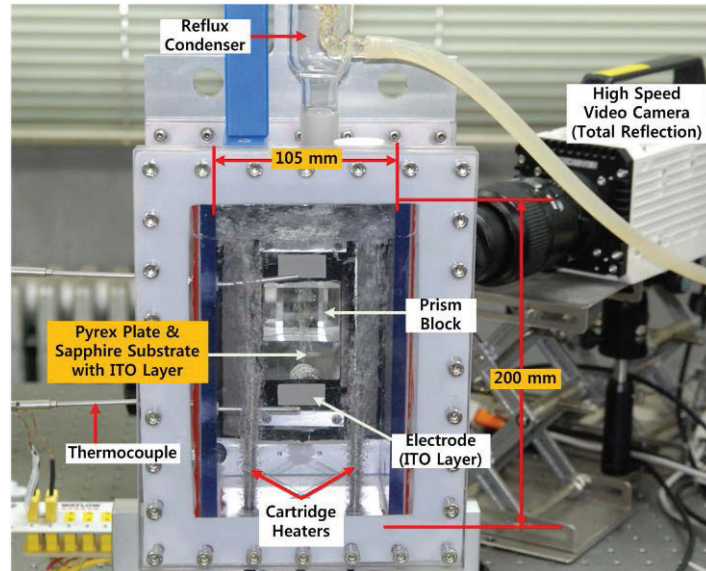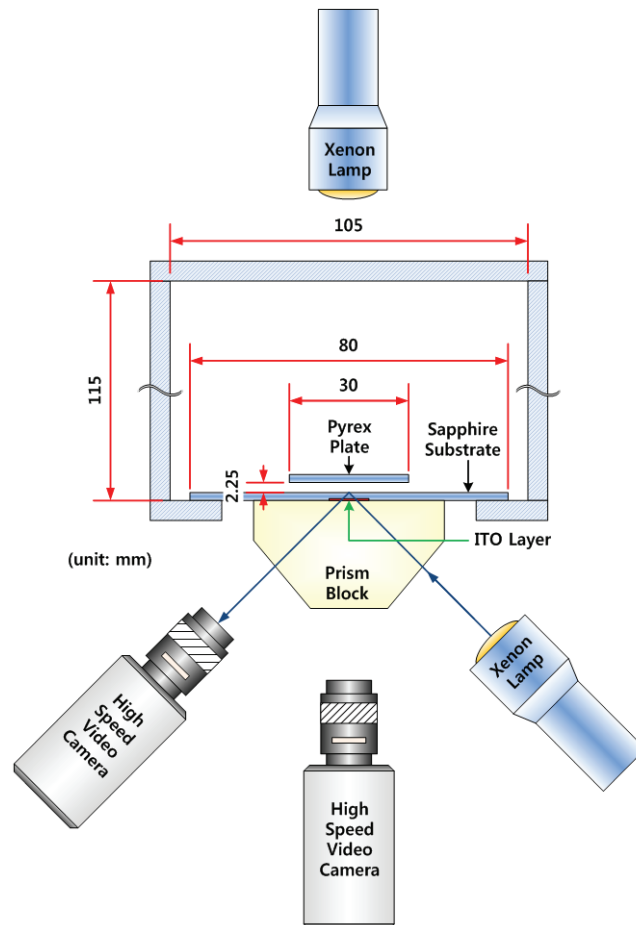
**Figure 1.  Photo of the Boiling Pool.**



**Figure 2.  Schematic of the Test Apparatus Seen from the Top.**

Two different sets of experiments were conducted separately. In the first set of experiments, the whole boiling area was visualized using only a shadowgraph technique in order to observe the macroscopic and global bubble behavior. Before the whole field visualization experiments, the CHF value was determined by the total reflection observation. The CHF value corresponded to the heat flux at which a non-rewetting dry area appeared as in the works of Chu et al. [13]. The whole field visualization experiments were conducted at seven heat flux levels from 30.9% CHF to 97.5% CHF conditions. In the second set of experiments, the visualization was focused on the smaller region at the upper part of the ITO heater in order to observe the local bubble behavior and the rewetting characteristics in a more detailed way. The synchronized total reflection and shadowgraph technique was applied to this local visualization experiments. The local field visualization experiments were conducted at eight heat flux levels from 46.3% CHF to 100% CHF conditions. Among those heat flux conditions, the whole field and local field visualization experiments were performed at the same five heat flux conditions, which ranged from 61.7% CHF to 97.5% CHF conditions. The visualization areas of each set of experiments are shown in Fig. 3. The total reflection and shadowgraph images were recorded at a frame rate of 10,000 fps for all experiments.
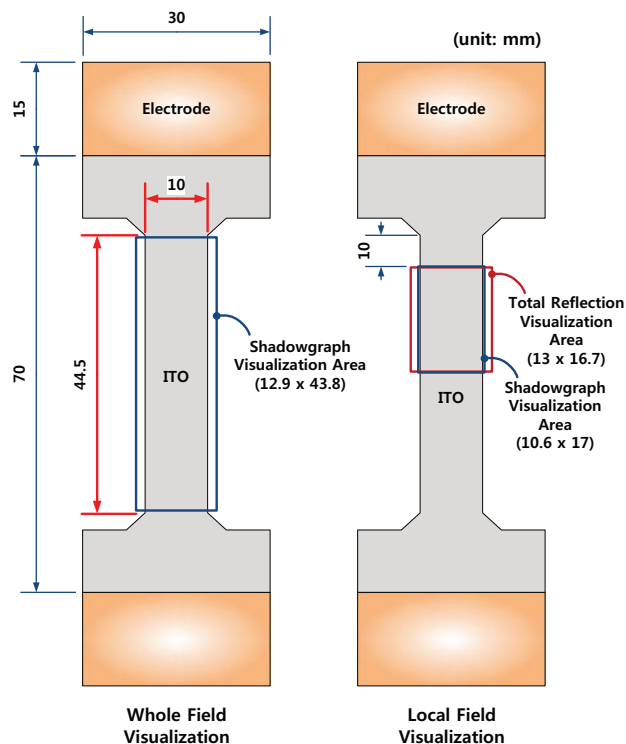


**Figure 3. Schematic of the ITO Layer and the Areas of Visualization.**

## 3. RESULTS AND DISCUSSION

### 3.1. Results of the Whole Field Visualization Experiments

A periodic feature of a slug flow was clearly observed in the shadowgraph images above the heat flux of 77.2% CHF. That is, (1) a massive slug bubble is initially formed by multiple steps of cascading coalescence among a lot of bubbles at the bottom part of the ITO heating region, (2) the slug bubble moves upward by buoyancy and the size of the slug bubble becomes bigger due to additional coalescence with the bubbles which exist at the downstream, (3) the slug bubble is followed by the slug tail region where discrete bubbles are mixed with a liquid flow, and (4) the next cycle of the slug bubble and slug tail

region is formed on the heating surface after the former slug bubble and slug tail disappear from the boiling surface.

As the heat flux increases, the following changes were observed in the global boiling structures: (1) The size of the slug bubble increases owing to the enhancement of the bubble nucleation activity, (2) the discrete bubble regime in the slug tail region transforms gradually to the continuous bubbly layer regime, and it is also due to the enhancement of the bubble nucleation activity on the heating surface, and (3) the distance between the aft of the slug tail region and the front of the next slug bubble becomes closer, and they are connected to each other at the heat flux level between 92.6% CHF and 97.5% CHF. As a result, a continuous gas phase exists over the total length of the heating surface along its central axis.

Global boiling structures in the present narrow vertical channel submerged in a pool of saturated Freon R-113 are presented in Figs. 4-6, which corresponds to the heat flux levels of 77.2% CHF, 92.6% CHF, and 97.5% CHF, respectively.
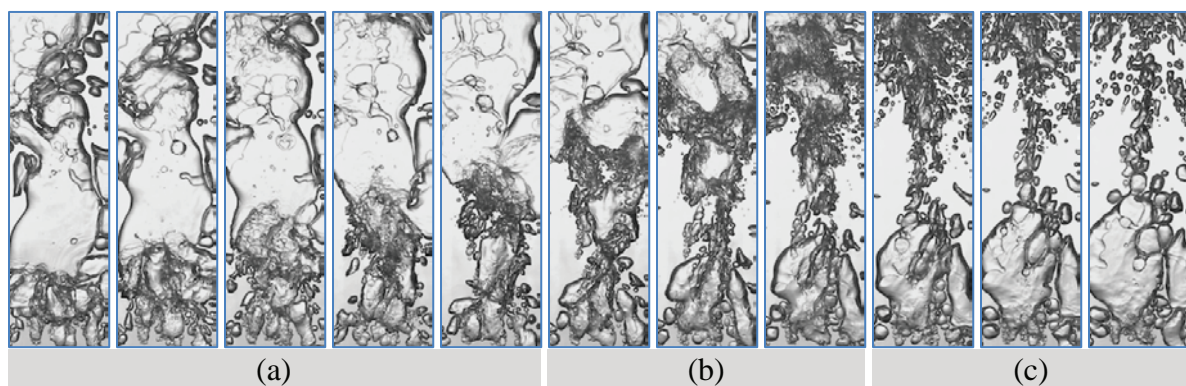


(a)                                        (b)                                        (c)

**Figure 4. Whole Field Visualization Images for Global Boiling Structure at 77.2% CHF (125 kW/m$^2$): (a) Formation of a Slug Bubble and Its Upward Movement; (b) Rewetting of the Large Dry Patch by the Slug Tail Region; (c) Formation of the Next Cycle Slug Bubble; Time Interval between Each Image Is 5 msec.**
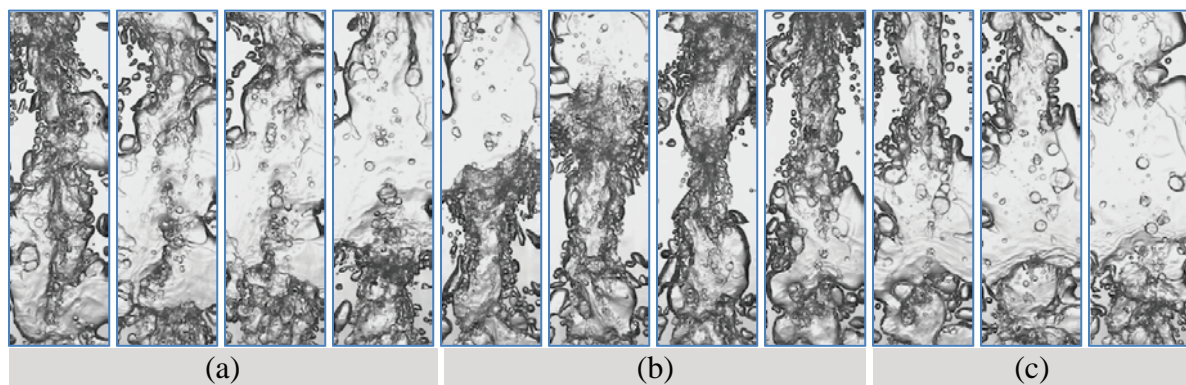


(a)                                        (b)                                        (c)

**Figure 5. Whole Field Visualization Images for Global Boiling Structure at 92.6% CHF (150 kW/m$^2$): (a) Formation of a Slug Bubble and Its Upward Movement; (b) Rewetting of the Large Dry Patch by the Slug Tail Region, and the Connection between the Aft of the Slug Tail Region and the Front of the Next Cycle Slug Bubble; (c) Formation of the Next Cycle Slug Bubble; Time Interval between Each Image Is 10 msec.**
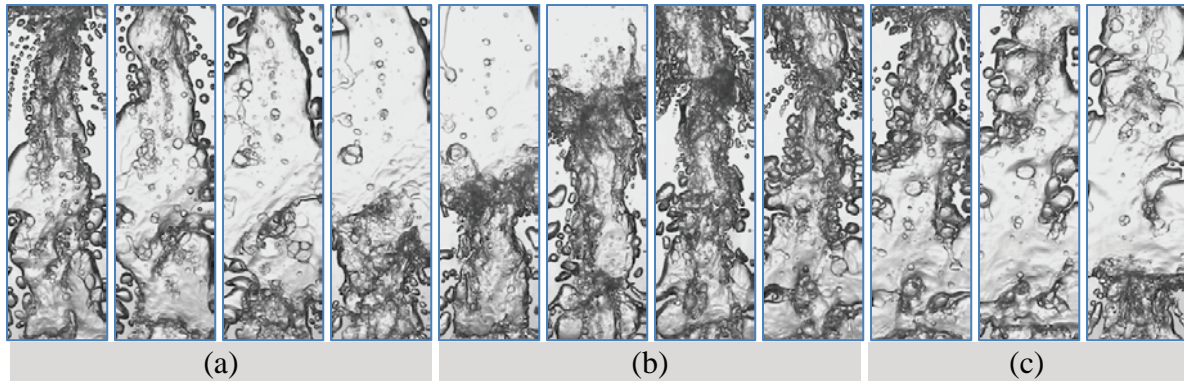
**Figure 6. Whole Field Visualization Images for Global Boiling Structure at 97.5% CHF (158 kW/m²): (a) Formation of a Slug Bubble and Its Upward Movement; (b) Rewetting of the Large Dry Patch by the Slug Tail Region; (c) Formation of the Next Cycle Slug Bubble; Time Interval between Each Image Is 10 msec.**

### 3.2. Results of the Local Field Visualization Experiments and Suggestion of CHF Mechanism

More detailed local boiling structures, dynamic behavior of the dry area, and the rewetting process were observed by the synchronized visualization of the total reflection and shadowgraph over the upper part of the heating surface (Figs. 7-10). Based on this observation, the CHF mechanism is suggested for saturated pool boiling in a vertical narrow gap.

According to the total reflection images in Figs. 7-10, not only the size of the slug bubble but also the size of the dry patch under the slug bubble increases as the heat flux increases. The heating surface under the slug bubble is almost dry above the heat flux level of 77.2% CHF. However, the large dry patch under the slug bubble is almost completely rewetted as the slug tail region rushes into the region covered by the slug bubble (Fig. 7 (b)). This is the time when and the location where the heating surface has a minimum dry area fraction. In other words, the maximum cooling of the heat surface occurs at this time and location.

The following changes occur gradually in the rewetting process of the large dry patch as the heat flux increases: (1) The flow regime in the front area of the slug tail region transforms from a discrete bubble regime to a continuous bubbly layer regime, (2) dry spots and dry patches appear under the bubbly layer of the front area of the slug tail region owing to the enhanced bubble nucleation activity and evaporation capability when the slug tail region rushes into the large dry patch under the slug bubble. As a result, the rewetting efficiency of the slug tail region for the large dry patch decreases, and the minimum dry area fraction becomes higher, and (3) The aft of the slug tail region and the front of the next slug bubble becomes connected to each other, and the dry area fraction in this region increases along with the increase of the heat flux.

With a further increase of the heat flux, a non-rewetting region appears even when the front area of the slug tail region rushes into the large dry patch under the slug bubble. This region is marked by the rectangle in Fig. 10 (b). This non-rewetting region remains non-rewetted when the rear area of the slug tail region and the next cycle slug bubble pass this region because the maximum rewetting of the heat surface occurs by the front area of the slug tail region. The occurrence of this non-rewetting region is due to the enhancement of the bubble nucleation activity and evaporation capability in the bubbly layer of the slug tail region.
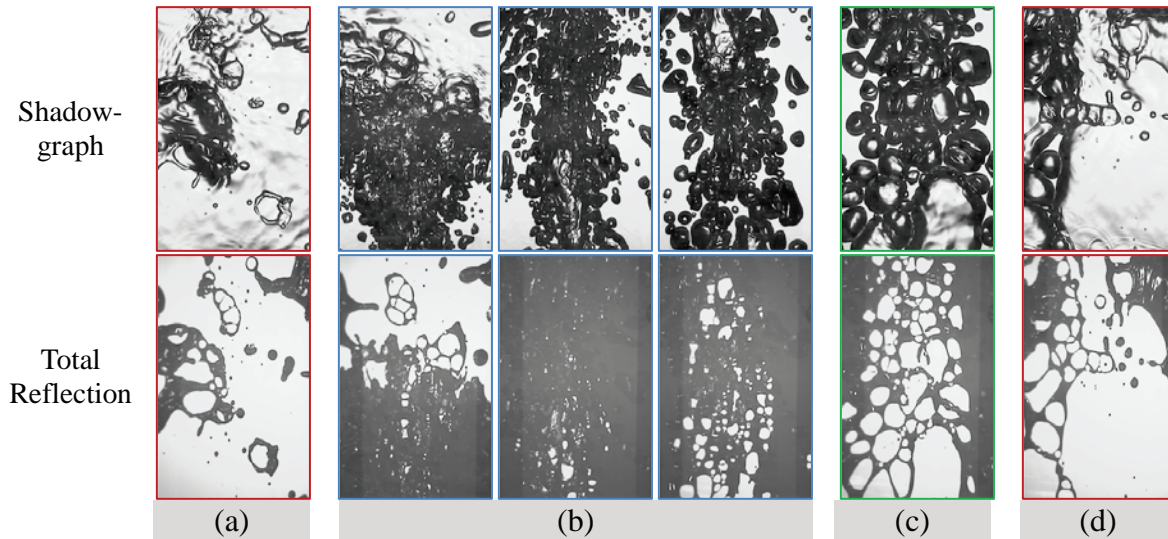
**Figure 7. Local Field Visualization Images of Synchronized Total Reflection and Shadowgraph at 77.2% CHF (125 kW/m$^2$): (a) Dry Patch under the Slug Bubble; (b) Rewetting of the Dry Patch by the Slug Tail Region; (c) Dry Areas at the Upstream of under the Next Cycle Slug Bubble; (d) Dry Patch under the Next Cycle Slug Bubble.**
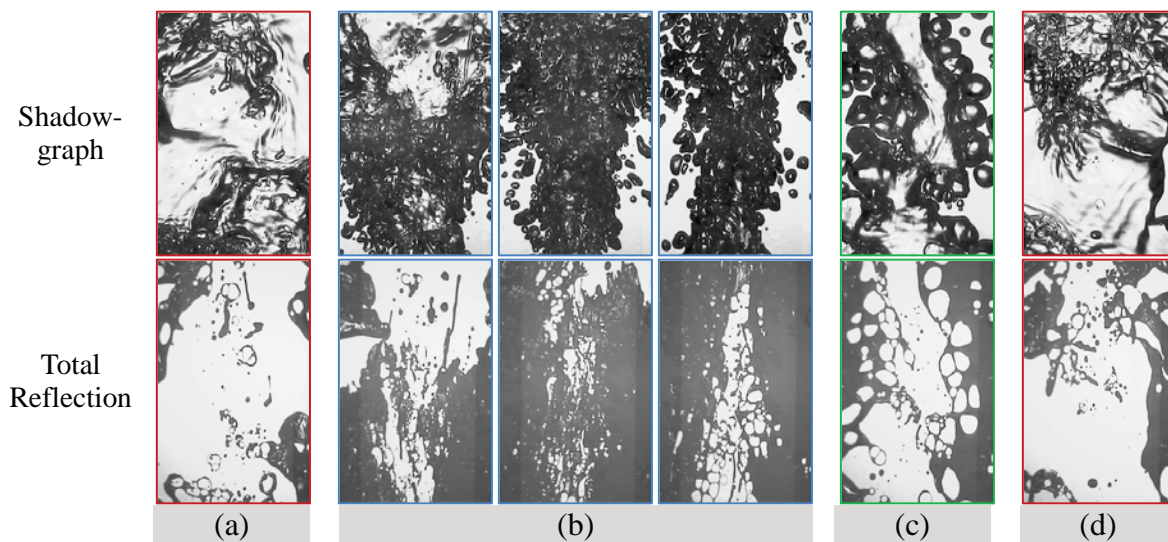


**Figure 8. Local Field Visualization Images of Synchronized Total Reflection and Shadowgraph at 92.6% CHF (150 kW/m$^2$): (a) Dry Patch under the Slug Bubble; (b) Rewetting of the Dry Patch by the Slug Tail Region; (c) Dry Areas at the Upstream of under the Next Cycle Slug Bubble; (d) Dry Patch under the Next Cycle Slug Bubble.**

**Figure 9. Local Field Visualization Images of Synchronized Total Reflection and Shadowgraph at 97.5% CHF (158 kW/m$^2$): (a) Dry Patch under the Slug Bubble; (b) Rewetting of the Dry Patch by the Slug Tail Region; (c) Dry Areas at the Upstream of under the Next Cycle Slug Bubble; (d) Dry Patch under the Next Cycle Slug Bubble.**
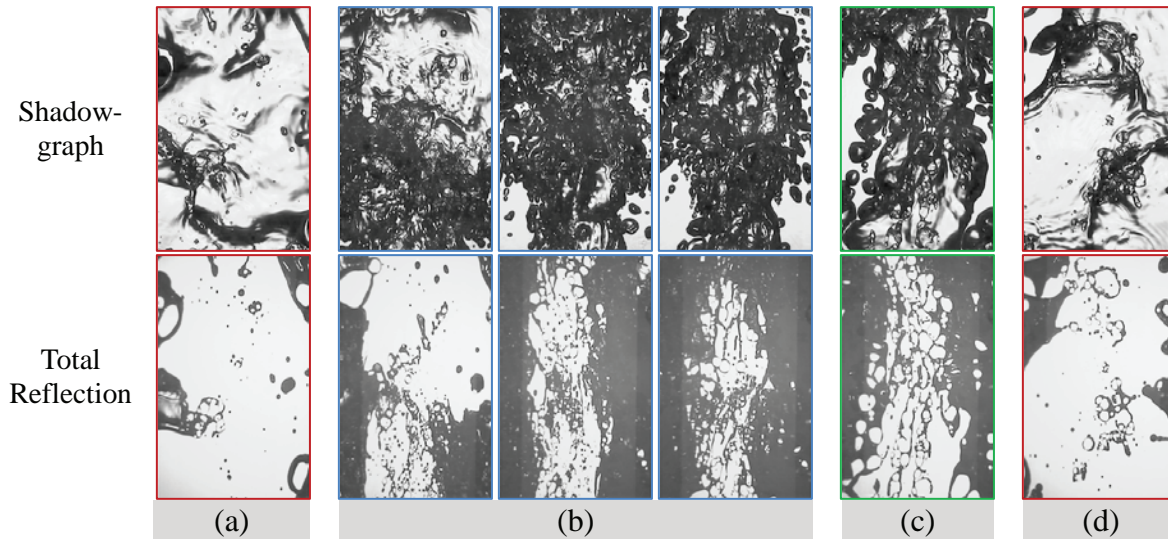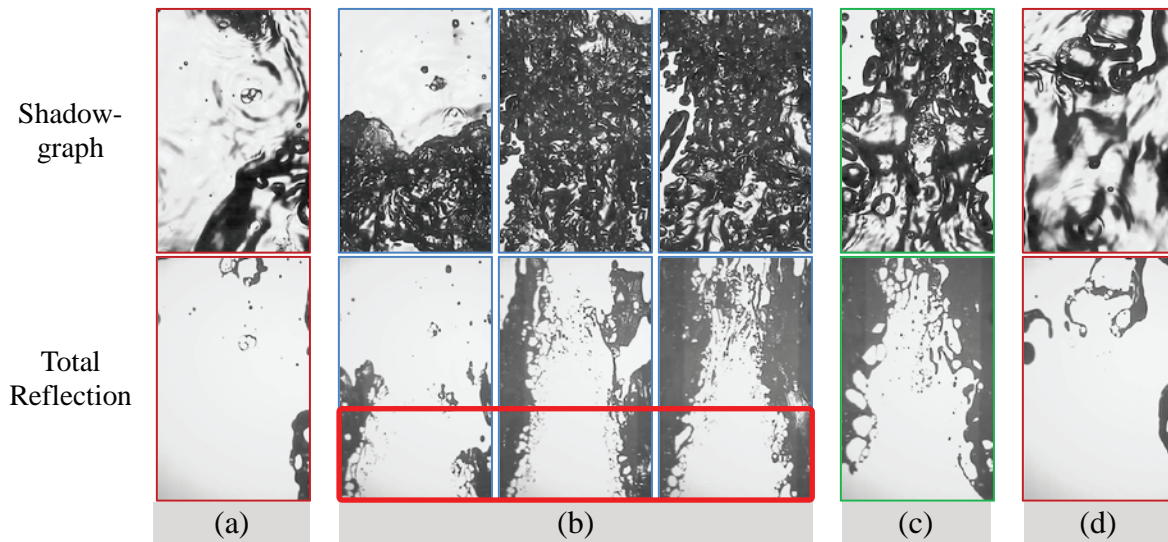


**Figure 10. Local Field Visualization Images of Synchronized Total Reflection and Shadowgraph at CHF Condition (162 kW/m$^2$): (a) Dry Patch under the Slug Bubble; (b) Appearance of the Non-Rewetting Area in the Slug Tail Region; (c) Sustentation of the Non-Rewetting Dry Area at the Upstream of under the Next Cycle Slug Bubble; (d) Dry Patch under the Next Cycle Slug Bubble.**

If this non-rewetting region is sustained for many cycles of slug bubble formation, the local heating surface temperature under this region will increase continuously, and will thus eventually lead to a burnout of the heating surface. For the horizontal pool boiling of the saturated water experiments of Chu et al. [13], a massive bubble formed and departed from the heating surface as the heat flux approached the CHF value. At the CHF condition, a small non-rewetting dry area appeared and became increasingly larger as the number of cycles for the formation of a massive bubble increased. Finally, the non-rewetting dry area covered the whole heating surface (8 mm × 18 mm) after about four seconds elapsed from its first appearance. Therefore, the condition for the CHF occurrence corresponded to the condition for the appearance of the non-rewetting dry area. In the present study, the heater power was tripped and

disconnected when the non-rewetting dry area was observed for several cycles of the slug bubble formation in order to protect the heater from a burnout.

In the present experimental condition of saturated Freon R-113 pool boiling in a vertical narrow gap, the cooling of the heating surface at a high heat flux condition was governed by the rewetting capability of the slug tail region for the large dry patch under the slug bubble. Therefore, the critical heat flux occurred when the dry area formation capability (*i.e.*, bubble nucleation activity and evaporation capability) in the bubbly layer of the slug tail region overwhelmed the rewetting capability of the slug tail region for the large dry patch.

CHF mechanisms in the literature such as 'liquid sublayer dryout models' of Lee and Mudawwar [4] and Haramura and Katto [3] do not correctly describe the present observations. These models postulate that CHF is triggered when a liquid layer between a vapor blanket and a heating surface dries out during the hovering time of the vapor blanket. However, the formation of the large dry patch under the slug bubble is a necessary condition for CHF but not the direct cause of the CHF occurrence in the present boiling configuration. CHF is triggered by the degradation of the rewetting capability of the slug tail region for the large dry patch formed under the slug bubble.

## 4.  CONCLUSIONS

In-depth visualization studies were made to observe the global and local boiling structures, dynamic behavior of the dry area, and its rewetting process in a vertical narrow channel submerged in a pool of saturated Freon R-113. Based on this observation, new CHF mechanism was suggested for the present boiling configuration.

The periodic feature of a slug flow prevailed above the heat flux of 77.2% CHF. The heating surface under the slug bubble was almost dry, but this large dry patch was effectively rewetted as the slug tail region rushed into the region covered by the slug bubble. The heating surface had a minimum dry area fraction at this moment. In other word, the cooling of the heating surface was governed by the rewetting capability of the slug tail region.

The dry area fraction in the slug tail region increased gradually with an increase in the heat flux, and the rewetting efficiency of the slug tail region became deteriorated owing to an enhancement of the bubble nucleation activity and evaporation capability in the slug tail region. A non-rewetting region appeared in the slug tail region and sustained for several cycles of slug bubble formation when the dry area formation capability in the slug tail region overwhelmed the rewetting capability of the slug tail region, which corresponded to the CHF occurrence.

### REFERENCES

1.  S. Nukiyama, "The Maximum and Minimum Values of the Heat Q Transmitted from Metal to Boiling Water under Atmospheric Pressure," *International Journal of Heat and Mass Transfer*, **9**, pp. 1419-1433 (1966).
2.  N. Zuber, *Hydrodynamic Aspects of Boiling Heat Transfer*, Ph.D. Dissertation, Research Laboratory, Los Angeles and Ramo-Wooldridge Corporation, University of California, Los Angeles, CA (1959).

3.  Y. Haramura and Y. Katto, "New Hydrodynamic Model of Critical Heat Flux Applicable Widely to Both Pool and Forced Convection Boiling on Submerged Bodies in Saturated Liquids," *International Journal of Heat and Mass Transfer*, **26**, pp. 379-399 (1983).

4.  C.H. Lee and I. Mudawwar, "A Mechanistic Critical Heat Flux Model for Subcooled Flow Boiling Based on Local Bulk Flow Condition," *International Journal of Multiphase Flow*, **14**, pp. 711-728 (1988).

5.  C. Unal, V. Daw, and R.A. Nelson, "Unifying the Controlling Mechanisms for the Critical Heat Flux and Quenching: The Ability of Liquid to Contact the Hot Surface," *Journal of Heat Transfer*, **114**, pp. 972-982 (1992).

6.  C.O. Gersey and I. Mudawar, "Effects of Heater Length and Orientation on the Trigger Mechanism for Near-Saturated Flow Boiling Critical Heat Flux–II. Critical Heat Flux Model," *International Journal of Heat and Mass Transfer*, **38**, pp.643-654 (1995).

7.  A.H. Howard and I. Mudawar, "Orientation Effects on Pool Boiling Critical Heat Flux (CHF) and Modeling of CHF for Near-Vertical Surfaces," *International Journal of Heat and Mass Transfer*, **42**, pp. 1665-1688 (1999).

8.  S. G. Kandlikar, "A Theoretical Model to Predict Pool Boiling CHF Incorporating Effects of Contact Angle and Orientation," *Journal of Heat Transfer*, **123**, pp. 1071-1079 (2001).

9.  C.-K. Guan, J. F. Klausner, R. Mei, A new mechanistic model for pool boiling CHF on horizontal surfaces," *International Journal of Heat and Mass Transfer*, **54**, pp. 3960-3969 (2011).

10. S. Nishio, T. Gotoh, and N. Nagai, "Observation of Boiling Structures in High Heat-Flux Boiling," *International Journal of Heat and Mass Transfer*, **41**, pp. 3191-3201 (1998).

11. H.J. Chung and H.C. NO, "Simultaneous Visualization of Dry Spots and Bubbles for Pool Boiling of R-113 on a Horizontal Heater," *International Journal of Heat and Mass Transfer*, **46**, pp. 2239-2251 (2003).

12. I.-C. Chu, H.C. NO, and C.-H. Song, "Visualization of Boiling Structure and Critical Heat Flux Phenomenon for a Narrow Heating Surface in a Horizontal Pool of Saturated Water," *International Journal of Heat and Mass Transfer*, **62**, pp. 142-152 (2013).

13. I.-C. Chu, H.C. NO, C.-H. Song, and D.J. Euh, "Observation of Critical Heat Flux Mechanism in Horizontal Pool Boiling of Saturated Water," *Nuclear Engineering and Design*, **279**, pp. 189-199 (2014).

14. H.D. Kim and J. Buongiorno, "A Novel Infrared-Based Experimental Technique to Detect Phase Dynamics on Boiling Surface," *Proceedings of the 14th International Topical Meeting on Nuclear Reactor Thermalhydraulics (NURETH-14)*, Toronto, Ontario Canada, NURETH-14-16 (2011).

15. T.G. Theofanous, T.N. Dinh, J.P. Tu, A.T. Dinh, "The Boiling Crisis Phenomenon Part II: Dryout Dynamics and Burnout," *Experimental Thermal and Fluid Science*, **26**, pp. 793-810 (2002).

16. C.D. Gerardi, *Investigation of the Pool Boiling Heat Transfer Enhancement of Nano-Engineered Fluids by Means of High-Speed Infrared Thermography*, PhD thesis, Massachusetts Institute of Technology, Cambridge, MA (2009).

17. M. Misale, G. Guglielmini, and A. Priarone, "HFE-7100 Pool Boiling Heat Transfer and Critical Heat Flux in Inclined Narrow Spaces," *International Journal of Refrigeration*, **32**, pp. 235-245 (2009).